Supplementary Materials for

Additive manufacturing of multi-metallic materials to achieve multi-functionality

Xiao Shang[1†], Evelyn Li[1†], Soumya S. Dash[1], Ajay Talbot[1], and Yu Zou[1*]

*Corresponding author. Email: mse.zou@utoronto.ca

† These authors contributed equally to this work

This PDF file includes:

Figures. S1 to S5
Tables S1 to S3
Movies S1 to S2
References (1 to 3)

Other Supplementary Materials for this manuscript include the following:

Movies S1 to S2

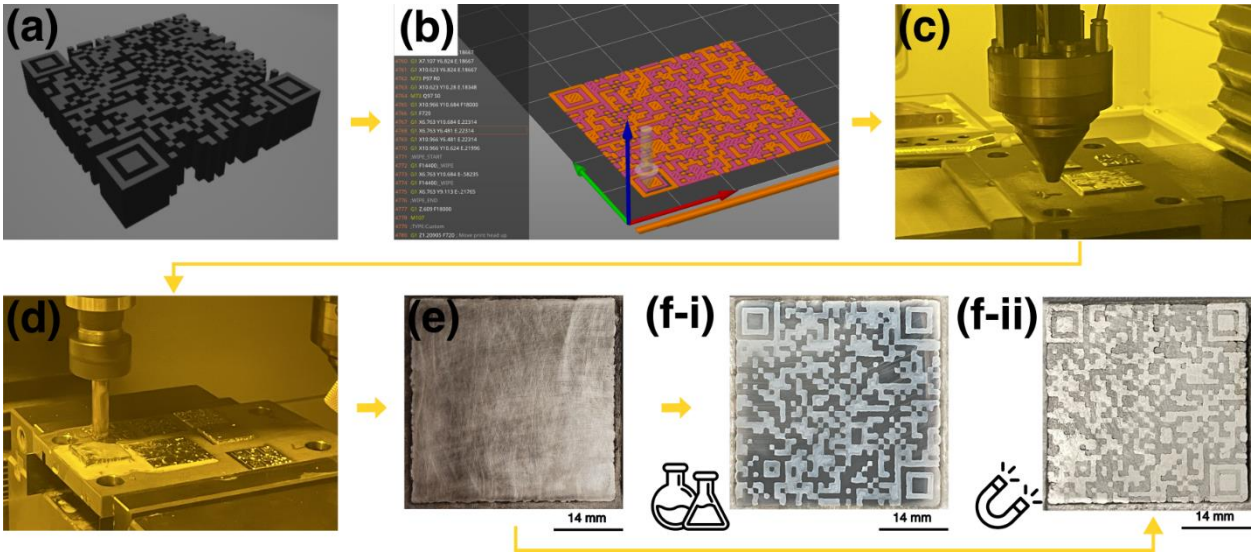

Figure S1 The manufacturing and decryption processes of the multi-functional materials (MFMs) for information encoding. (a) Encoding information into the original quick response (QR) code in the form of a stereolithography (.stl) computer aided design (CAD) model file. **(b)** Convert the .stl model into a series of G-codes while adding directed energy deposition (DED) process information including laser power, printing speed, multi-material switching etc. **(c)** Printing the samples using an in-house developed DED machine. **(d)** and **(e)** Post-process the as-printed samples by CNC machining and griding. **(f-i)** Decrypting the QR code using chemical etching reagent. **(f-ii)** Decrypting the QR code using magnetic particles.

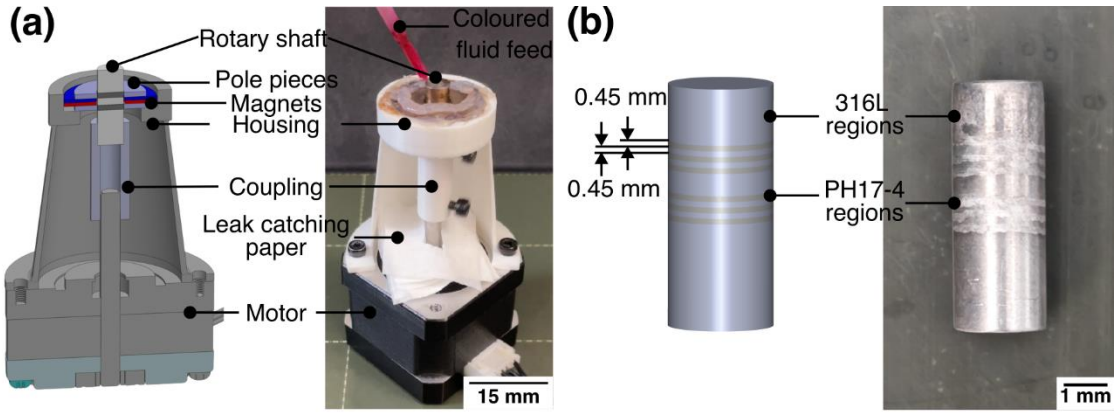

Figure S2 A setup simulating a vacuum rotary motion feedthrough implementing the redesigned ferrofluidic seal system using a MFM shaft. (a) Detailed design of the setup with all major components labelled. On the left is a CAD model giving a cross-sectional view of the setup, and on the right is the setup in real-life. **(b)** The designed and the printed MFM shaft. On the left is the CAD model with dimensions of the shaft, and on the right is the MFM shaft in real-life.

This setup is designed to simulate a typical vacuum feedthrough implementing the ferrofluidic seal. Nickel alloy 400 washers were used to function as pole pieces, and a ring-shaped NdFeB permanent magnet was used to provide the magnetic field to form the ferrofluidic O-rings. To hold the washers and the magnet in place while leaving a gap for sealing between them and the rotary shaft, a housing was designed and printed using Polylactic acid (PLA) on a Prusa MK3S FDM printer. A coupler was designed and printed using the same method to couple the motor shaft and the MFM shaft, for conveying rotary motion. The seal tests were done by dropping and observing if coloured ink can pass through the gap intended to be sealed between the shaft and the pole pieces. The ink was a mixture of water and regular red ink for added visibility. The seal-ability under three conditions, i.e., static shaft, shaft rotation at 125 rpms, and shaft rotation at 625 rpms, were performed and compared with when no ferrofluidic O-ring was applied. Ferrofluid sourced from Applied Magnets was then applied at the gap between washer and shaft to create the ferrofluidic O-ring. Note that pressurized seal-ability of the MFM setup wasn't tested, considering that the seal-ability under pressure is more dependent on factors such as the machining quality of the components (*1*), the quantity of ferrofluid volume injection (*2*), the physical properties of the ferrofluid (*3*) etc., which are independent from the MFM shaft improvement proposed in this work.

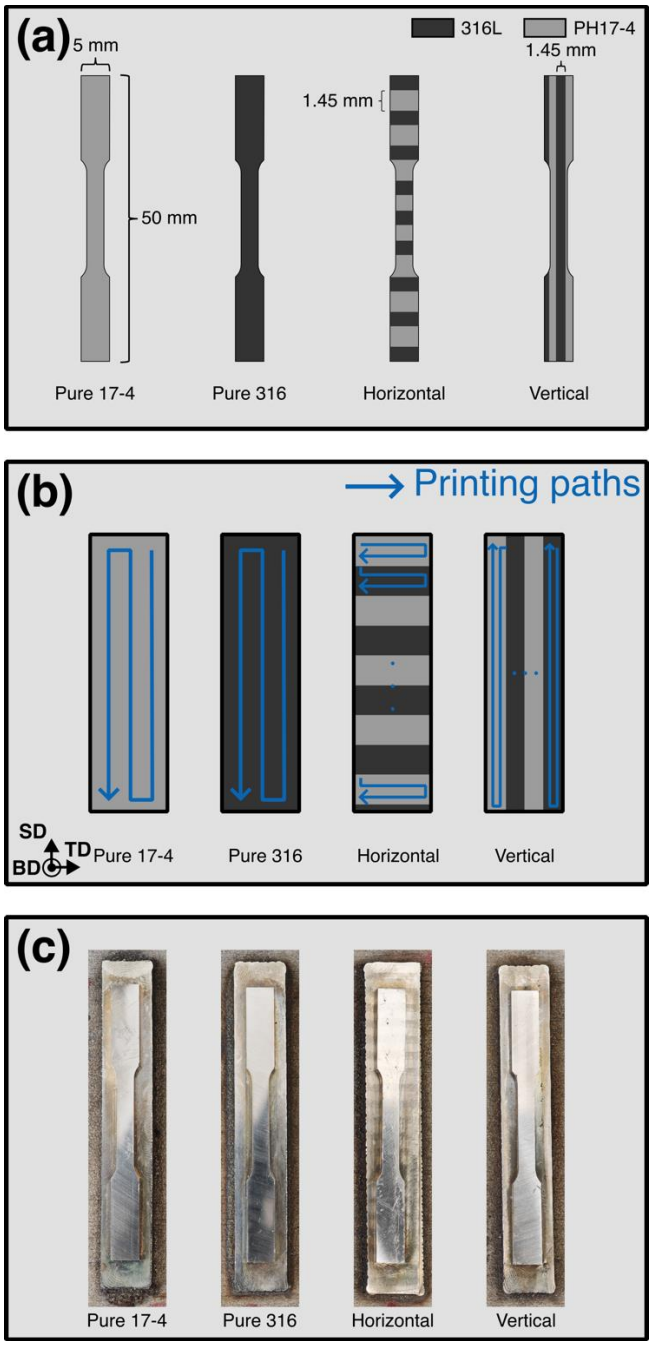

Figure S3 The MFM samples used in the mechanical testing. (a) Detailed designs of the tensile coupons being tested with dimensions marked. **(b)** Printing paths for making the cubes from which the tensile coupons were extracted. For all samples, the prints were done in a "zigzag" manner. For the two pure samples and the vertical sample, the long edge of the "zigzag" pattern is along the scan direction (SD). For the horizontal sample, the long edge of the "zigzag" pattern is along the transverse direction (TD). When fabricating the horizontal and vertical samples, two tracks were deposited in each material section before switching materials. **(c)** The tensile coupons after machining from the printed cubes.

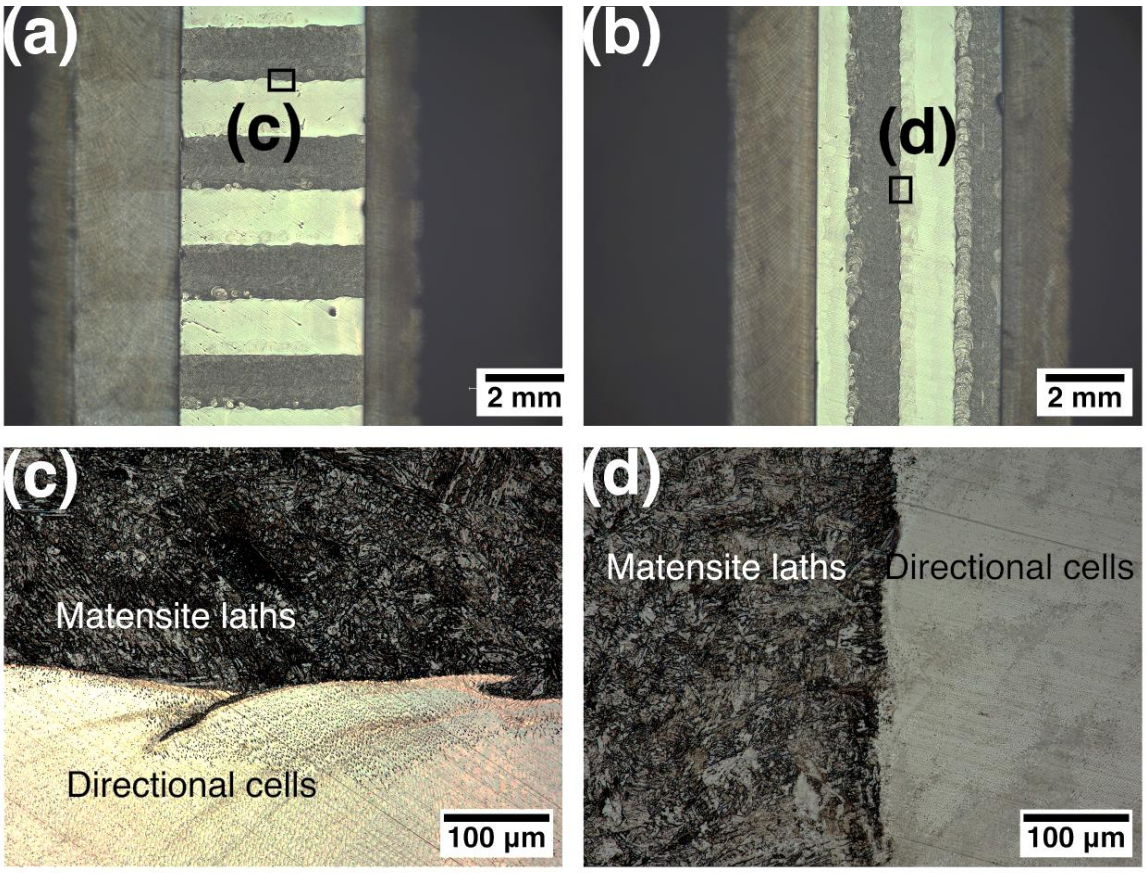

Figure S4 Etched horizontal and vertical samples. (a) and **(b)** Horizontal and vertical samples under a low magnification, showing the interface lines. **(c)** and **(d)** Horizontal and vertical samples under a high magnification, showing the microstructural features.

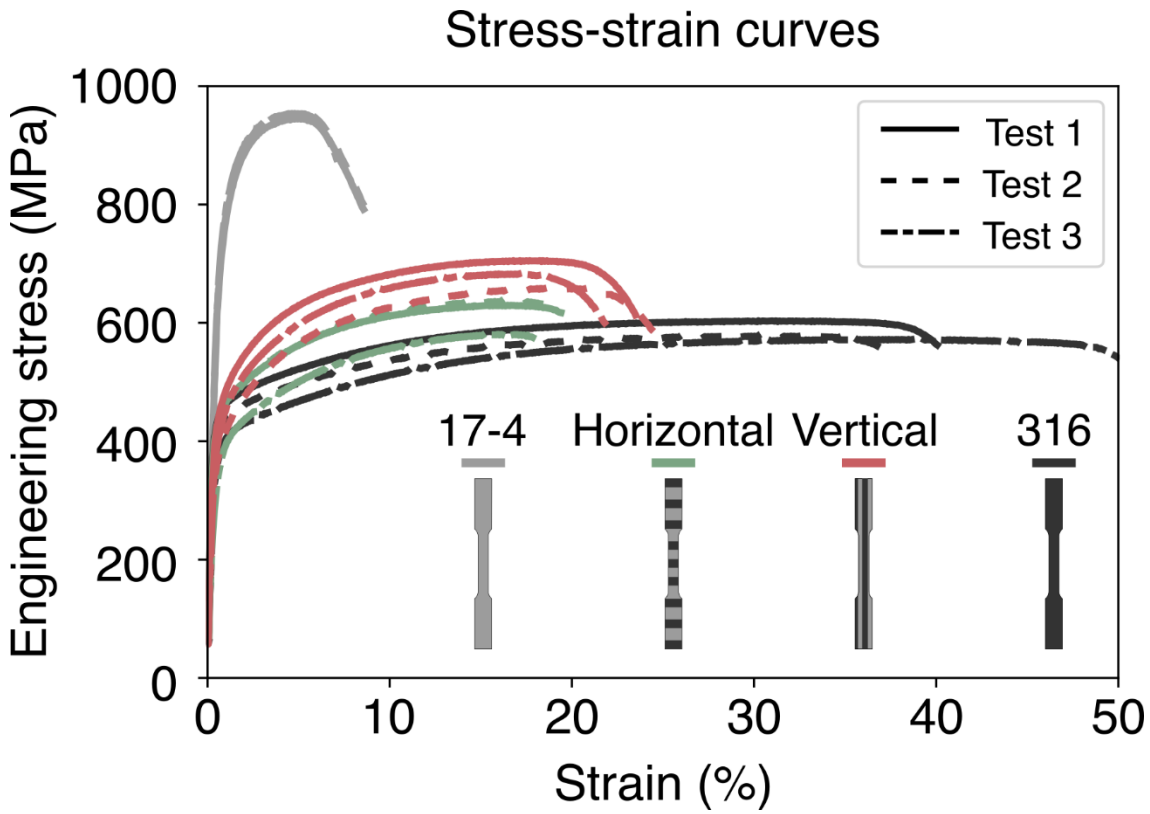

Figure S5 Stress-strain curves for all samples tested in the tensile tests. Each test was repeated three times for statistically meaningful results.

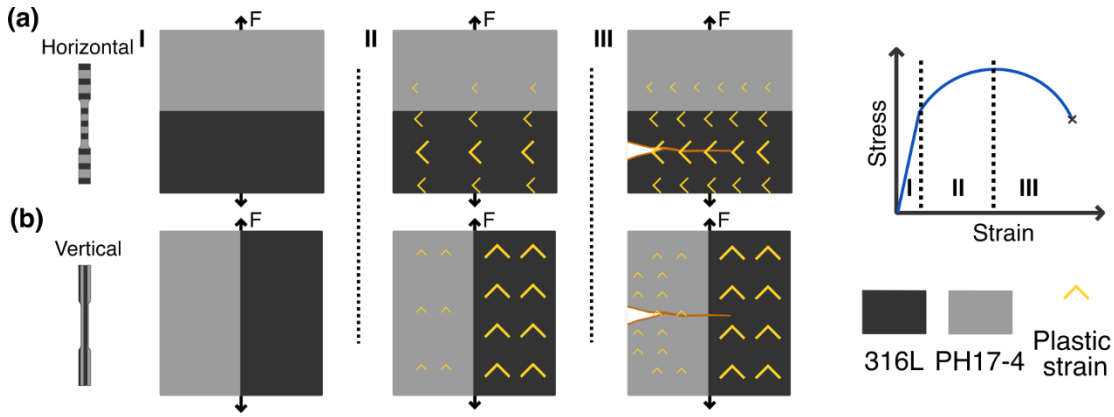

Figure S6 Schematics explaining the deformation mechanism. (a) and **(b)** are Schematics providing explanations on the deformation mechanisms of the horizontal and vertical samples, respectively. The three stages I, II, and III correspond to the elastic deformation (I), uniform plastic deformation (II), and non-uniform plastic deformation (III), as indicated in the stress-strain curve sketch. Plastic strains are represented with yellow arrows. The numbers and sizes of the yellow arrows indicate the density and size of the plastic strain, respectively.

Figure S6 (a) explains the deformation mechanism for the horizontal MFM samples. The deformation process is divided into three stages, i.e., the elastic deformation stage (I), the uniform plastic deformation stage (II), and the non-uniform plastic deformation stage (III). After the initial elastic (equal stress) stage I, in stage II the plastic strain accumulates, with higher plastic strains on the softer 316L regions. Such plastic strains decrease gradually from the 316L regions towards the 316L-PH17-4 interface, and eventually disappear on the pure PH17-4 regions, where only elastic strains exist. In stage III, the plastic strains on the 316L regions continue to accumulate non-uniformly as necking develops. Cracks initiates at this stage and cause the samples to fracture.

Figure S6 (b) explains the deformation mechanism for the vertical MFM samples. In stage I, no plastic deformation is being generated and the whole sample is in an equal strain state. Moving to stage II, the regions with softer 316L deforms more severely, evening out the plastic strains in the PH17-4 regions and delaying necking. In stage III, necking happens and cracks initiate from the accumulated plastic strains in the PH17-4 regions and fracture the sample. It should be noted that, however, despite the improved *UTS* and ε_{max}, the yield strength (σ_y) for both the MFMs decrease compared to the pure samples (**Supplementary Table S1**).

Table S1. Test results on the mechanical properties of the pure alloy samples and MFM samples.

	Pure 17-4	**Pure 316**	**Horizontal**	**Vertical**
Ultimate tensile strength - *UTS* (MPa)	949.77±5.24	584.26±16.76	615.48±30.41	681.65±23.25
Elongation at break - ε_{max} (%)	8.07±0.86	42.32±6.61	18.72±0.83	23.24±1.39
Yield strength - σ_y (MPa)	701.10±5.05	392.68±19.41	376.09±46.41	377.00±37.35
Young's modulus - *E* (GPa)	130.01±3.13	127.51±20.22	131.63±14.22	133.64±13.57
***E* (GPa) by Voigt model**	NA	NA	130.86	NA
***E* (GPa) by Reuss model**	NA	NA	NA	130.85

Table S2. Chemical composition of the metal powders used in this work.

Material	Fe	Cr	Ni	Mo	C	N	Cu	Nb + Ta
SS 316L	Bal.	17.00-19.00	13.00-15.00	2.25-3.00	0-0.03	0-0.10	NA	NA
PH17-4	Bal.	17.00	4.50	NA	<0.07	NA	4.00	0.3

Table S3. Process parameters used for sample generation in this work

MFMs	Laser power (W)	Scan speed (mm/s)	Hatch spacing (ratio to track width)	Resolution (mm)
Discs	300	8	0.5	-
QR code (coarse module)	300	8	0.6	0.914
QR code (fine module)	440	12	0.7	0.625
Ferrofluidic seal shaft	440	4	0.6	-
Mechanical testing coupons	450	4	0.74	-

Movie S1.

Magnetic decryption process of the MFM QR code samples with low and high module densities, respectively.

Movie S2.

Seal-ability test of the MFM redesigned ferrofluidic seal setup under static and dynamic conditions.

References

1. K. van der Wal, R. A. J. van Ostayen, S. G. E. Lampaert, Ferrofluid rotary seal with replenishment system for sealing liquids. *Tribology International* **150**, 106372 (2020).
2. Y. Chen *et al.*, Experiment and Simulation on the Ferrofluid Boundary Deformation and Fluctuation Characters of a High-Speed Rotary Seal. *Journal of Tribology* **146**, (2024).
3. M. Szczech, W. Horak, Tightness testing of rotary ferromagnetic fluid seal working in water environment. *Industrial Lubrication and Tribology* **67**, 455-459 (2015).